




Actuating water droplets on liquid infused surfaces: A rickshaw for droplets

Christophe Raufaste ^{1,2} Simon J. Cox ³ and Franck Celestini ^{1,*}

¹Université Côte d'Azur, CNRS, Institut de Physique de Nice, 06100 Nice, France

²Institut Universitaire de France (IUF), 75005 Paris, France

³Department of Mathematics, Aberystwyth University, Aberystwyth SY23 3BZ, United Kingdom



(Received 27 April 2021; accepted 20 July 2021; published 11 August 2021)

We investigate the dynamics of millimeter-sized droplets moved on a liquid infused surface. The motion of the droplet is driven by a small spherical bead, whose trajectory is precisely controlled, which acts as a carrier. We first characterize the strength of the contact that maintains the adhesion between the droplet and the bead as a function of the ratio R/r of their radii. When the bead is moved at a fixed velocity, the droplet follows its trajectory until a critical value of the velocity is reached at which the bead and the droplet lose contact. The critical velocity is rationalized as a balance between the capillary contact force and the friction acting on the droplet where it is in contact with the substrate. Experimental results are in good agreement with the model proposed. This study highlights a very efficient actuation method for millimetric droplets.

DOI: [10.1103/PhysRevFluids.6.083603](https://doi.org/10.1103/PhysRevFluids.6.083603)

I. INTRODUCTION

The control and actuation of liquid droplets in contact with a substrate is fundamental to the development of milli- and microfluidic devices [1] and surface cleaning technology [2,3]. Surface energy gradients [4], thermal gradients [5], chemical reactions [6], or electric fields [7,8] can displace droplets with velocities up to 1 cm s^{-1} . Nevertheless, full control of the droplet is often a very difficult task due to the lateral adhesion exerted by the substrate associated with pinning at defects. This results in contact angle hysteresis [9], enhanced dissipation [10,11], and nonlinear features analogous to solid friction [12], which require elegant actuation strategies such as vibration of the substrate [13–17].

In order to promote mobility and simplify droplet manipulation, the gap between the solid substrate and the moving drop can be lubricated in a manner inspired by plants with slippery surfaces [18,19]. Textured lubricant infused surfaces [20–26] or smooth lubricant coated slippery surfaces [27–31] can be designed with appropriate surface engineering and display spectacular slippery behaviors with negligible hysteresis [32].

Biswas *et al.* [33] have demonstrated that accurate motion and complex drop trajectories can be achieved with magnetic substrates whose topography can be modulated with an external electromagnetic field. Similarly, textured lubricant infused surfaces can be impregnated with ferrofluids for active manipulation of droplets with a magnetic field [34,35].

In this article we demonstrate that both accurate and complex trajectories, as well as high velocities—up to 0.6 m s^{-1} —can be achieved using a bead as a carrier, like a rickshaw, for the droplet. The bead is controlled by a magnet placed under the substrate: The method is nonintrusive and allows complex trajectories described by the trajectory of the magnet. In this system, the control of the droplet is effective as long as the droplet does not detach from the bead.

*Franck.Celestini@univ-cotedazur.fr

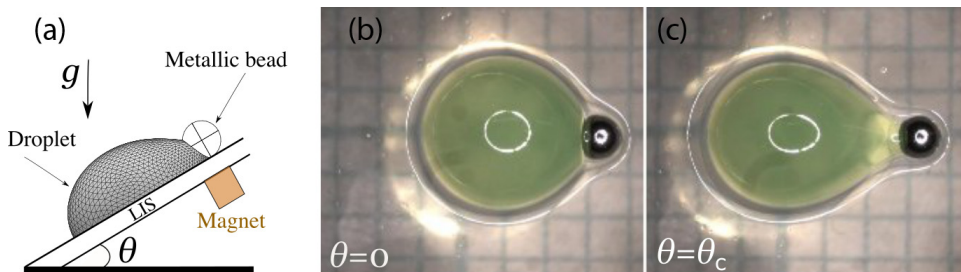


FIG. 1. (a) Representation of the system on an inclined plane. Two images taken from above in the reference frame of the substrate for $\theta = 0$ (b) and at the critical inclination θ_c (c), respectively ($r = 0.5$ mm and $R = 2$ mm).

This article is organized in two parts. First, we study experimentally and numerically the integrity of the contact between the bead and the droplet, and the maximal force that can be sustained in the particular geometry of interest. Second, we characterize the maximal velocity at which the drop can be moved with such a system, which corresponds to the dynamical breaking of the bead/droplet contact and the detachment of the drop. We show that this limit is imposed by the friction law between the droplet and the substrate.

II. GEOMETRY OF INTEREST

The basic geometry consists of a layer of polydimethylsiloxane (PDMS), approximately 1 mm thick, laid on a flat aluminum substrate. The layer of PDMS was initially impregnated by immersion in a bath of silicon oil of viscosity $\eta_o = 5.1$ mPa s for 24 h. With such a protocol, there is always a thin layer of silicon oil remaining at the surface of the PDMS. A steel bead is deposited on the PDMS and its position is controlled with a cylindrical neodymium magnet (10 mm in diameter and height) placed below the substrate. We have chosen beads with radii r between 0.5 and 1.5 mm.

One droplet of de-ionized water (density $\rho = 1000$ kg m⁻³ and viscosity $\eta_w = 1.0$ mPa s) is deposited with a high-precision syringe pump at the contact between the bead and the PDMS substrate. If its typical size is below the capillary length, its shape is quasihemispherical due to an apparent contact angle close to 90° [22–24]. Therefore, we define its radius R from the volume of a hemisphere and its mass is given by $m = \rho \frac{2}{3} \pi R^3$. A small amount of fluorescein salt is added to the water to improve the quality of the images. The surface tensions are estimated to be around $\gamma_{o,a} = 20$ mN m⁻¹ for the oil-air interface [36] and around $\gamma_{o,w} = 35$ mN m⁻¹ for the oil-water interface [37]. We write $\gamma = \gamma_{o,a} + \gamma_{o,w}$ for the effective surface tension at the surface of the water droplet since it is “cloaked” by a thin film of silicon oil [23].

III. INTEGRITY OF THE BEAD/DROPLET CONTACT

A. Experiments

The integrity of the bead/droplet contact is tested by subjecting the system to gravity, $g = 9.81$ m s⁻². This is realized with an inclined plane, whose angle θ can be increased from 0° to 50° (Fig. 1). As the angle is increased from 0°, the droplet is stretched by gravity but remains in contact with the bead and the contact area decreases. We define θ_c to be the critical angle at which detachment occurs, which is displayed in Fig. 2(a). For a given bead radius r , the larger the drop, the smaller is θ_c . We find that $\sin(\theta_c)$ increases linearly with the reciprocal of the volume, $\sin(\theta_c) \propto 1/R^3$. The larger the bead radius, the larger is the coefficient of proportionality between $\sin(\theta_c)$ and $1/R^3$. In our range of parameters, the coefficient of proportionality appears to depend linearly on r so that we propose the scaling $\sin(\theta_c) \propto \gamma r / \rho g R^3$ to describe the experimental results [Fig. 2(b)].

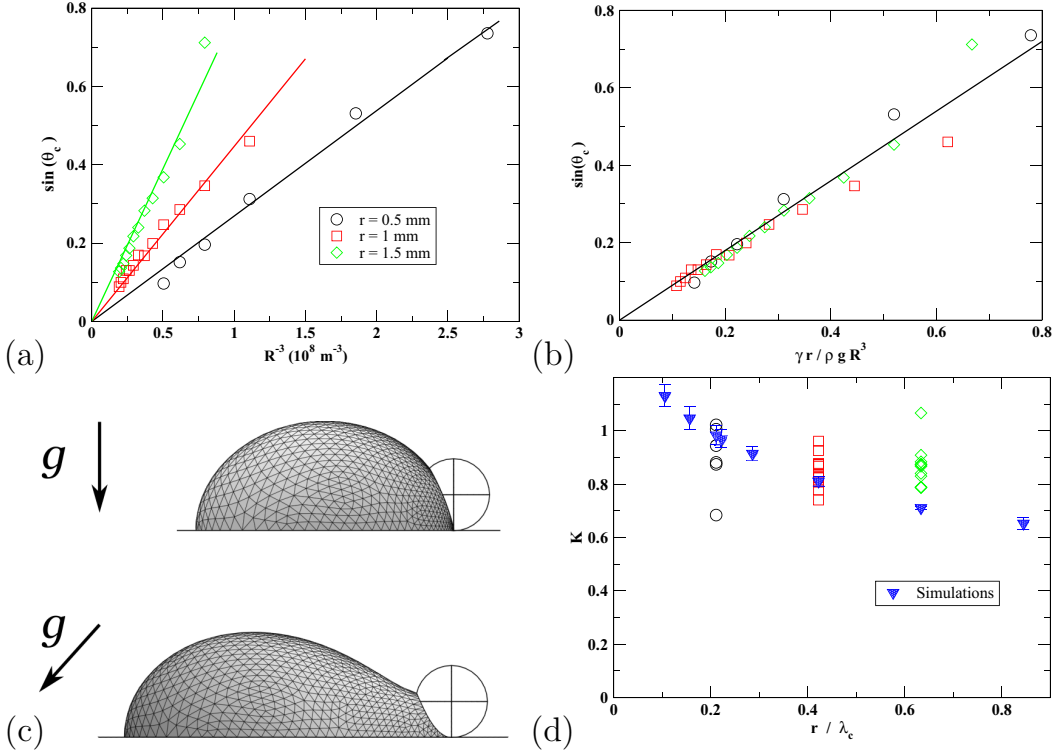


FIG. 2. K analysis in experiments and simulation. (a) $\sin(\theta_c)$ as a function of R^3 in experiments for beads of radius 0.5 (black circles), 1 (red squares), and 1.5 mm (green diamonds). Proportionality relations are displayed by solid lines. (b) Same data with $\sin(\theta_c)$ as a function of $\gamma r / \rho g R^3$ with $\gamma = 55 \text{ mN m}^{-1}$. (c) Snapshots from the simulation for $\theta = 0^\circ$ and 42° , respectively. (d) K as a function of r / λ_c for both experiments and simulations. In simulation, each point corresponds to one value of r / λ_c and roughly 100 values of R / λ_c , whose effect is quantified by the error bars.

B. Dimensional analysis

In the pendant drop geometry, the determination of the detachment force is a long-standing problem tackled by Lord Rayleigh in 1899 [38], and more recently reviewed by Eggers [39]. The particular case of detachment from a sphere has been considered in the context of a particle attached to a liquid interface [40,41]. Detachment is intrinsically linked to the collapse of the liquid neck that connects the drop to the sphere. Using dimensional analysis, we can write a generic expression for the detachment force in the form

$$\frac{2\pi}{3} K \gamma r, \quad (1)$$

where r is the sphere radius, γ the surface tension, and the factor $2\pi/3$ is added for convenience. With $\lambda_c = \sqrt{\gamma / \rho g}$ denoting the capillary length, K is a dimensionless function that depends only on r / λ_c and R / λ_c if the contact angle is constant (fixed at 90° in what follows).

In our particular geometry of a drop attached to a spherical bead of radius r in contact with a surface tilted at an angle θ , detachment occurs when the liquid neck cannot support the effective weight $mg \sin(\theta)$ of a drop of mass $m = \rho(2\pi/3)R^3$. As a consequence, K is inferred from the measurement of the critical angle θ_c as

$$K = \sin(\theta_c) \frac{\rho g R^3}{r \gamma} = \sin(\theta_c) \frac{R^3}{r \lambda_c^2}. \quad (2)$$

In what follows we study $K(r/\lambda_c, R/\lambda_c)$.

C. Simulations

We now probe the effect of these two dimensionless quantities with numerical simulations.

The SURFACE EVOLVER software [42] allows us to find the static shape of a droplet for different bead sizes, different droplet sizes and surface tensions, and different surface inclinations. The contact angles between the droplet and the bead and between the droplet and the substrate are set to 90° . We discretize the surface of the droplet, as in Fig. 2(c), and constrain its boundary to lie either on the inclined surface or attached to the bead, including the weight of the droplet as an integral over its surface. The triangulation is refined four times and, for each set of parameters r and γ , we use just over 1000 gradient-descent steps with occasional Hessian iterations (using second derivative information) to find a local minimum of surface area, checking the eigenvalues of the Hessian matrix to ensure stability [43]. We then slowly increase the drop volume (in steps of 1 mm^3) or increase the surface inclination θ (by changing the direction of gravity, in steps of 0.1°), again seeking a minimum of surface area, until the surface becomes unstable (measured through a change in sign of the smallest eigenvalue).

In the simulations, γ is varied between 20 and 100 mN m^{-1} , r between 0.25 and 2 mm, and R between 0.8 and 4 mm. This leads to values of r/λ_c and R/λ_c between 0.1 and 0.9 and between 0.5 and 1.8, respectively. The ranges tested are significantly larger than what is expected in experiments to check the robustness of the trends. In Fig. 2(d), K is plotted as a function of r/λ_c and a clear trend is found: K is almost independent of R/λ_c , the effect of which is measured by the size of the error bars.

D. Discussion

As expected from Fig. 2(b), K is almost constant in experiments, and we measure $K_{\text{expt}} = 0.87 \pm 0.08$ on average. The slight dispersion [Fig. 2(d)] is associated with experimental errors and to a small deviation from linearity. The comparison with the simulations is good too, with the difference that K_{sim} is found to decrease slightly from 1 to 0.7 in our parameter range. In fact, differences between the experimental and numerical approaches might exist. As an example, the substrate is soft in experiments and the bead can be slightly displaced with respect to the flat surface. In what follows, we take $K = K_{\text{expt}}$ constant in Eq. (1) to characterize the detachment force in our setup.

IV. CRITICAL VELOCITY ANALYSIS

A. Experiments

We now probe the maximal velocity of the drop with such a system. To do this, the system is mounted on a rotating device [Figs. 3(a) and 3(b)]. The radial distance a of the magnet from the axis of rotation is fixed at 40 mm and the rotation frequency Ω is typically varied between 0.2 and 2 rotations per second. In this setup, the magnet, the bead, and the droplet are fixed and the substrate moves with a velocity $V = \Omega a$ at the droplet position. In the typical procedure, Ω is increased slowly and we record the critical value at detachment, Ω_c . In our parameter range we found critical velocities $V_c = \Omega_c a$ between 0.06 and 0.55 m s^{-1} . In this procedure, the radii of both the bead and the droplet are varied. Looking for a scaling, we found that all the data collapse on a single curve by plotting V_c as a function of R/r [Fig. 3(c)]. The law can be well fitted by an exponent $-3/2$ but V_c seems to saturate for $R/r \lesssim 1$.

B. Model

Even though droplets on lubricated surfaces exhibit negligible hysteresis of the contact angle, they are subject to friction. Keiser *et al.* [25] have shown different regimes of dissipation depending on the contrast of viscosity between the two liquid phases. If $\eta_o < \eta_w$ they have shown that

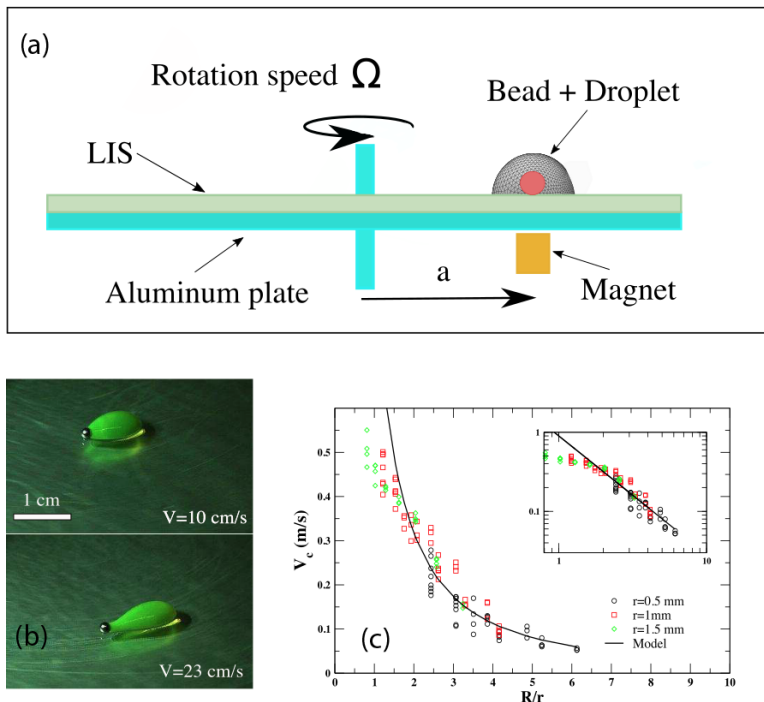


FIG. 3. (a) Rotating setup designed to determine the critical velocity. (b) Snapshots taken for two velocities (the lower one is taken just prior to detachment). (c) Critical velocity V_c as a function of R/r . Inset: log-log scale. The solid line is a power-law interpolation (exponent $-3/2$, prefactor 0.85 m s^{-1}).

dissipation for a millimeter-sized drop remains classical (Stokes-like). In the other limit $\eta_o > \eta_w$ dissipation mainly occurs in the oil and a nonlinear friction law, with a force proportional to $V^{2/3}$, is observed consistent with dissipation in the oil meniscus surrounding the droplet [44]. In this case, only the projected length of the meniscus in the direction perpendicular to the flow, estimated as $2R$, contributes to dissipation. Regarding our viscosity contrast ($\eta_o \simeq 5\eta_w$), we assume dissipation in the oil meniscus and the following expression for the friction force:

$$F_{\text{vis}} = \xi \gamma' \text{Ca}^{2/3} 4R. \quad (3)$$

Here, $\xi \approx 6$ is a parameter whose exact value depends on the nature of the motion of the meniscus interface [44], γ' is the surface tension at the free interface of the meniscus [since oil is in contact with both air and water, we take the average value $\gamma' = (\gamma_{o,a} + \gamma_{o,w})/2 = \gamma/2$ as the effective surface tension for calculations], and $\text{Ca} = \eta_o V / \gamma'$ is the capillary number. From the detachment analysis performed in Sec. III, we have measured that the maximal force the bead/droplet contact can sustain is given by $(2\pi/3)K\gamma r$ [Eq. (1)]. If we balance these two forces, we obtain an estimate of the critical velocity:

$$V_c = \frac{\gamma}{\eta_o} \left(\frac{K}{\xi} \right)^{3/2} \frac{\pi^{3/2}}{3^{3/2}} \left(\frac{R}{r} \right)^{-3/2} \approx (0.33 \text{ m s}^{-1}) \left(\frac{R}{r} \right)^{-3/2}. \quad (4)$$

In experiments, we found a proportionality factor of 0.85 m s^{-1} [Fig. 3(c)]. We conclude that our estimate is in good agreement with the data given the approximations. In fact, it is not clear how the presence of the bead affects dissipation in the meniscus, particularly in the regime $R/r < 1$ where we observe a saturation of the velocity. In this regime, the capillary number may reach $\text{Ca} \sim 0.1$, contradicting the assumption $F_{\text{vis}} \propto \text{Ca}^{2/3}$, which is only true in the limit $\text{Ca} \ll 1$.

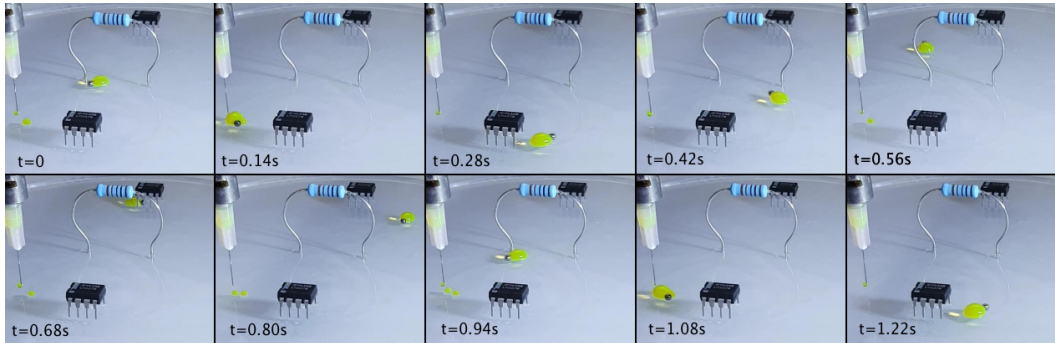


FIG. 4. Image sequence of a complex trajectory performed by a millimetric droplet. The circuit has a figure of eight shape and its length of about 10 cm is traveled in about 2 s. See movies in the Supplemental Material [45].

V. CONCLUSION

In summary, we have demonstrated an efficient and accurate way to actuate droplets on liquid infused surfaces. This method allows droplets to perform fast, precise, and complex trajectories at the same time. The method presented here with millimeter-sized droplets could be further developed to transpose the principle to smaller scales for microfluidic applications.

Our combined theoretical, numerical, and experimental analysis clarifies the way in which the droplet and bead interact. We determine the maximum force that the bead can exert on the droplet before detachment, and from our analysis we conclude that dissipation limits the maximal velocity reached by the system. In particular, we measure characteristics that emphasize dissipation inside the meniscus surrounding the droplet, in agreement with earlier work [25,46].

Finally, we illustrate the high precision and velocity achieved by this system in Fig. 4: The droplet is forced to perform a figure of eight shape in about 2 s. For this experiment the magnet is guided using an xy plotter. We estimate the typical length of the circuit to be 10 cm. Two movies are given in the Supplemental Material [45] with two different periods of 2 and 1 s, respectively.

ACKNOWLEDGMENTS

W. Bontemps and V. Dorel are thanked for their input at the beginning of the project.

-
- [1] J. Genzer and R. R. Bhat, Surface-bound soft matter gradients, *Langmuir* **24**, 2294 (2008).
 - [2] T. Heckenthaler, S. Sadhujan, Y. Morgenstern, P. Natarajan, M. Bashouti, and Y. Kaufman, Self-cleaning mechanism: Why nanotexture and hydrophobicity matter, *Langmuir* **35**, 15526 (2019).
 - [3] A. Naga, A. Kaltbeitzel, W. S. Y. Wong, L. Hauer, H.-J. Butt, and D. Vollmer, How a water drop removes a particle from a hydrophobic surface, *Soft Matter* **17**, 1746 (2021).
 - [4] M. K. Chaudhury and G. M. Whitesides, How to make water run uphill, *Science* **256**, 1539 (1992).
 - [5] J. B. Brzoska, F. Brochard-Wyart, and F. Rondelez, Motions of droplets on hydrophobic model surfaces induced by thermal gradients, *Langmuir* **9**, 2220 (1993).
 - [6] C. D. Bain, G. D. Burnett-Hall, and R. R. Montgomerie, Rapid motion of liquid drops, *Nature (London)* **372**, 6505 (1994).
 - [7] M. G. Pollack, R. B. Fair, and A. D. Shenderov, Electrowetting-based actuation of liquid droplets for microfluidic applications, *Appl. Phys. Lett.* **77**, 1725 (2000).
 - [8] O. D. Velev, B. G. Prevo, and K. H. Bhatt, On-chip manipulation of free droplets, *Nature (London)* **426**, 6966 (2003).

- [9] J. F. Joanny and P. G. de Gennes, A model for contact angle hysteresis, *J. Chem. Phys.* **81**, 552 (1984).
- [10] C. Huh and L. E. Scriven, Hydrodynamic model of steady movement of a solid/liquid/fluid contact line, *J. Colloid Interface Sci.* **35**, 85 (1971).
- [11] J. H. Snoeijer and B. Andreotti, Moving contact lines: Scales, regimes, and dynamical transitions, *Annu. Rev. Fluid Mech.* **45**, 269 (2013).
- [12] N. Gao, F. Geyer, D. W. Pilat, S. Wooh, D. Vollmer, H.-J. Butt, and R. Berger, How drops start sliding over solid surfaces, *Nat. Phys.* **14**, 191 (2018).
- [13] S. Daniel, S. Sircar, J. Gliem, and M. K. Chaudhury, Ratcheting motion of liquid drops on gradient surfaces, *Langmuir* **20**, 4085 (2004).
- [14] S. Daniel, M. K. Chaudhury, and P.-G. de Gennes, Vibration-actuated drop motion on surfaces for batch microfluidic processes, *Langmuir* **21**, 4240 (2005).
- [15] P. Brunet, J. Eggers, and R. D. Deegan, Vibration-Induced Climbing of Drops, *Phys. Rev. Lett.* **99**, 144501 (2007).
- [16] X. Noblin, R. Kofman, and F. Celestini, Ratchetlike Motion of a Shaken Drop, *Phys. Rev. Lett.* **102**, 194504 (2009).
- [17] S. Mettu and M. K. Chaudhury, Motion of liquid drops on surfaces induced by asymmetric vibration: Role of contact angle hysteresis, *Langmuir* **27**, 10327 (2011).
- [18] H. F. Bohn, and W. Federle, Insect aquaplaning: Nepenthes pitcher plants capture prey with the peristome, a fully wettable water-lubricated anisotropic surface, *Proc. Natl. Acad. Sci. USA* **101**, 14138 (2004).
- [19] U. Bauer, H. F. Bohn, and W. Federle, Harmless nectar source or deadly trap: Nepenthes pitchers are activated by rain, condensation and nectar, *Proc. R. Soc. B* **275**, 259 (2008).
- [20] S. Anand, A. T. Paxson, R. Dhiman, J. D. Smith, and K. K. Varanasi, Enhanced condensation on lubricant-impregnated nanotextured surfaces, *ACS Nano* **6**, 10122 (2012).
- [21] A. K. Epstein, T.-S. Wong, R. A. Belisle, E. M. Boggs, and J. Aizenberg, Liquid-infused structured surfaces with exceptional anti-biofouling performance, *Proc. Natl. Acad. Sci. USA* **109**, 13182 (2012).
- [22] A. Lafuma, and D. Quéré, Slippery pre-suffused surfaces, *Europhys. Lett.* **96**, 56001 (2011).
- [23] J. D. Smith, R. Dhiman, S. Anand, E. Reza-Garduno, R. E. Cohen, G. H. McKinley, and K. K. Varanasi, Droplet mobility on lubricant-impregnated surfaces, *Soft Matter* **9**, 1772 (2013).
- [24] T.-S. Wong, S. H. Kang, S. K. Y. Tang, E. J. Smythe, B. D. Hatton, A. Grinthal, and J. Aizenberg, Bioinspired self-repairing slippery surfaces with pressure-stable omniphobicity, *Nature (London)* **477**, 443 (2011).
- [25] A. Keiser, L. Keiser, C. Clanet, and D. Quéré, Drop friction on liquid-infused materials, *Soft Matter* **13**, 6981 (2017).
- [26] A. Keiser, P. Baumli, D. Vollmer, and D. Quéré, Universality of friction laws on liquid-infused materials, *Phys. Rev. Fluids* **5**, 014005 (2020).
- [27] R. Pant, P. K. Roy, A. K. Nagarajan, and K. Khare, Slipperiness and stability of hydrophilic surfaces coated with a lubricating fluid, *RSC Adv.* **6**, 15002 (2016).
- [28] D. Daniel, J. V. I. Timonen, R. Li, S. J. Velling, and J. Aizenberg, Oleoplaning droplets on lubricated surfaces, *Nat. Phys.* **13**, 1020 (2017).
- [29] G. Zhang, B. Liang, Z. Zhong, Y. Huang, and Z. Su, One-step solvent-free strategy for covalently attached, substrate-independent transparent slippery coating, *Adv. Mater. Interfaces* **5**, 1800646 (2018).
- [30] M. Sharma, P. K. Roy, J. Barman, and K. Khare, Mobility of aqueous and binary mixture drops on lubricating fluid-coated slippery surfaces, *Langmuir* **35**, 7672 (2019).
- [31] M. Sharma, P. K. Roy, R. Pant, and K. Khare, Sink dynamics of aqueous drops on lubricating fluid coated hydrophilic surfaces, *Colloids Surf., A* **562**, 377 (2019).
- [32] D. P. Regan and C. Howell, Droplet manipulation with bioinspired liquid-infused surfaces: A review of recent progress and potential for integrated detection, *Curr. Opin. Colloid Interface Sci.* **39**, 137 (2019).
- [33] S. Biswas, Y. Pomeau, and M. K. Chaudhury, New drop fluidics enabled by magnetic-field-mediated elastocapillary transduction, *Langmuir* **32**, 6860 (2016).
- [34] K. S. Khalil, S. R. Mahmoudi, N. Abu-dheir, and K. K. Varanasi, Active surfaces: Ferrofluid-impregnated surfaces for active manipulation of droplets, *Appl. Phys. Lett.* **105**, 041604 (2014).

- [35] W. Wang, J. V. I. Timonen, A. Carlson, D.-M. Drotlef, C. T. Zhang, S. Kolle, A. Grinthal, T.-S. Wong, B. Hatton, S. H. Kang, S. Kennedy, J. Chi, R. T. Blough, M. Sitti, L. Mahadevan, and J. Aizenberg, Multifunctional derrofluid-infused surfaces with reconfigurable multiscale topography, *Nature (London)* **559**, 77 (2018).
- [36] F. Gollwitzer, I. Rehberg, C. A. Kruelle, and K. Huang, Coefficient of restitution for wet particles, *Phys. Rev. E* **86**, 011303 (2012).
- [37] F. Peters and D. Arabali, Interfacial tension between oil and water measured with a modified contour method, *Colloids Surf., A* **426**, 1 (2013).
- [38] L. Rayleigh, Investigations in capillarity: The size of drops. The liberation of gas from supersaturated solutions. Colliding jets. The tension of contaminated water-surfaces, *Philos. Mag.* **48**, 321 (1899).
- [39] J. Eggers, Nonlinear dynamics and breakup of free-surface flows, *Rev. Mod. Phys.* **69**, 865 (1997).
- [40] A. D. Scheludko and D. Nikolov, Measurement of surface tension by pulling a sphere from a liquid, *Colloid Polym. Sci.* **253**, 396 (1975).
- [41] O. Pitois and X. Chateau, Small particle at a fluid interface: Effect of contact angle hysteresis on force and work of detachment, *Langmuir* **18**, 9751 (2002).
- [42] K. A. Brakke, The surface evolver, *Exp. Math.* **1**, 141 (1992).
- [43] K. A. Brakke, The Surface Evolver and the stability of liquid surfaces, *Philos. Trans. R. Soc. A* **354**, 2143 (1996).
- [44] I. Cantat, Liquid meniscus friction on a wet plate: Bubbles, lamellae, and foams, *Phys. Fluids* **25**, 031303 (2013).
- [45] See Supplemental Material at <http://link.aps.org/supplemental/10.1103/PhysRevFluids.6.083603> for videos.
- [46] D. Daniel, J. V. I. Timonen, R. Li, S. J. Velling, M. J. Kreder, A. Tetreault, and J. Aizenberg, Origins of Extreme Liquid Repellency on Structured, Flat, and Lubricated Hydrophobic Surfaces, *Phys. Rev. Lett.* **120**, 244503 (2018).